Batteries & Supercaps

Research Article
doi.org/10.1002/batt.202400110

Chemistry Europe
European Chemical Societies Publishing

www.batteries-supercaps.org

Influence of Carbonisation Temperatures on Multifunctional Properties of Carbon Fibres for Structural Battery Applications

Ruben Tavano,*[a] Johanna Xu,[a] Claudia Creighton,[b] Fang Liu,[a] Bhagya Dharmasiri,[b] Luke C. Henderson,[b] and Leif E. Asp*[a]

Carbon fibres are multifunctional materials considered for the realisation of structural battery electrodes. Processing conditions affect the carbonaceous microstructure of carbon fibres. The microstructure dictates the fibre's mechanical properties, i.e. modulus and strength, as well as its electrochemical capacity. Here, carbon fibre processing conditions are investigated to identify the effect of carbonisation temperature on carbon fibre multifunctionality. Different thermal conditions during carbonisation are considered, while keeping the precursor material, applied tension, and oxidation temperature constant. The carbonaceous microstructure of fibres is investigated via wide-angle x-ray scattering (WAXS) and transmission electron microscopy (TEM) analyses to determine the effect of the carbonisation temperature. Mechanical and electrochemical tests are performed to characterise carbon fibre multifunctionality with respect to mechanical and electrochemical performance. A moderate trade-off between mechanical and electrochemical performance is demonstrated, where the elastic modulus and strength decrease and the electrochemical capacity increase with reduced carbonisation temperature. Here, for the studied temperature interval, the elastic modulus and strength is found to drop up to 7% with a 15% increase in capacity. Thus, fibres customised for targeted multifunctionality within a limited design space can be realised by careful selection of the processing conditions in conventional carbon fibre manufacture.

Introduction

Multifunctional materials have potential to revolutionise the field of energy storage in transportation. By integrating electrical energy storage into structural components, such as those used in electric vehicles, lightweight electrical vehicles with increased range can be achieved. A structural battery composite is a prime example of a multifunctional material. The structural battery can simultaneously store electric energy and carry mechanical loads. Thereby combined energy storage and structural efficiency are intrinsic to the material. The most common architecture for structural batteries consists of a thin-ply carbon fibre negative electrode stacked on a glass fibre separator and a positive electrode. All the layers are impregnated, and the circuit connected, by a structural battery electrolyte (SBE). In this application, the carbon fibres serve as the host for lithium, as electron conductor, and reinforcement.[1–6]

The use of carbon fibres to store lithium was recognized in the early 1990s, with Ruland identifying the potential of carbon fibres and the need to understand the relationship between microstructure and properties.[7] More recently, Snyder et al. showed that polyacrylonitrile (PAN)-based carbon fibres are more favourable for lithium-ion insertion than pitch-based carbon fibres, making them suitable for use as multifunctional negative electrodes.[8] Since commercial carbon fibres are designed as reinforcement material for composite materials, the relationship between process parameters, the resulting carbon fibre microstructure, and mechanical properties is well understood.[9,10] The relationship between electro-chemo-mechanical performance of the fibre and its carbonaceous microstructure is less well understood. Recent works by Jacques et al. and Duan et al. explore the effects of lithium insertion on the physical and mechanical properties of carbon fibres.[11–14] In further studies, Kjell et al. analysed the electrochemical capacities of widely used commercially available PAN-based carbon fibres,[15] while Hagberg et al. examined the capacity and columbic efficiency (CE) of intermediate modulus (IM) carbon fibres, including T800 and IMS65, in comparison to highly graphitized high modulus (HM) M60J carbon fibres, using high precision coulometry.[16] Better electrochemical capacity was observed for IM carbon fibres, compared to HM carbon fibres, but the reasons behind the different performance were unknown. Fredi et al. used high-resolution TEM and in situ Raman spectroscopy to explain the lithiation mechanism for

[a] R. Tavano, Dr. J. Xu, Prof. F. Liu, Prof. L. E. Asp
Industrial and Materials Science
Chalmers University of Technology
Maskingränd 1, 41258, Göteborg, Sweden
E-mail: ruben.tavano@chalmers.se
leif.asp@chalmers.se

[b] Dr. C. Creighton, Dr. B. Dharmasiri, Prof. L. C. Henderson
Institute for Frontier Materials
Deakin University
75 Pigdons Rd, 3216, Waurn Ponds, Australia

Supporting information for this article is available on the WWW under https://doi.org/10.1002/batt.202400110

T800, IMS65, and M60J fibres.[17] The results showed that IM carbon fibres (T800 and IMS65) insert lithium with a mechanism like that in amorphous carbon, with different performances between the two types of carbon fibres. In contrast, the HM carbon fibre inserted lithium with a staging mechanism resembling that in graphite.[17] The lower electrochemical capacity of the HM fibre was further explained by that the staging process was partly obstructed by defects present in the large crystals in the turbostratic graphitic structure observed in the HM carbon fibre. The difference in electrochemical capacity observed between the two IM carbon fibres was partially explained by Johansen et al. by considering the differences in the residual amount and type of heteroatoms found in the microstructure.[18] Specifically, they found that the nitrogen heteroatom configuration varies between the two IM fibres. The IMS65 was found to have a larger proportion of pyridinic and pyrrolic nitrogen (20.5 %), compared to 14.2 % found for the T800 fibre. Pyridinic and pyrrolic nitrogen are found at defects in the carbonaceous structure, and thereby provide sites for lithium to coordinate with the carbon atoms. The higher amounts of pyridinic and pyrrolic nitrogen, hence, offer a plausible explanation to the difference in capacity found for IMS65 and T800 fibres.[18]

To utilise the high multifunctional performance of IM fibres Asp et al. employed T800 fibres as the negative electrode in a laminated structural battery composite.[19] A structural battery composite cell with an energy density of 24 Wh kg^{-1} and an elastic modulus of 25 GPa was demonstrated. Xu et al. used three of these cells connected in series to make a multicell structural battery laminate, showing great potential for the realisation of larger multifunctional systems.[20] Recently, improvements to the manufacturing process of the structural battery composite cell were proposed by Siraj et al., who obtained significantly improved performance and repeatability of the cells.[21] A vacuum-assisted infusion process for the SBE was used and an energy density of 41.2 Wh kg^{-1} was reported.

Commercial carbon fibres are not designed for multifunctionality. They have merely been made to provide desired combinations of strength and stiffness. Furthermore, the use of commercially available carbon fibres for multifunctional applications is complicated, due to the lack of information on the utilised precursor and the processing parameters. In addition, the fibre surface is treated with a sizing without disclosure of the exact chemical composition. To address these limitations, Xu et al. made different carbon fibres from a PAN precursor altering the applied tension during the stabilisation stage.[22] Three different tension forces were applied (low tension at 720 cN, medium tension at 2300 cN and high tension at 3025 cN). Xu et al. evaluated the electrochemical capacity, and the elastic modulus and tensile strength of the fibres. Applying a lower tension during the stabilisation stage showed enhanced electrochemical capacity but reduced the tensile strength and modulus of the final carbon fibre. Conversely, a higher tension boosted the mechanical properties but significantly reduced the ability to store lithium ions. The different behaviour was connected to inherent differences in d-spacing, crystallite orientation, and crystallite size. The best-performing multifunctional carbon fibre was found to be the one manufactured with a medium tension. Thus, process induced microstructural variations allow for realisation of carbon fibres with tailored multifunctional properties for use in structural battery electrodes.

In the current study, the effect of the carbonisation temperature on microstructure and multifunctionality is investigated. Different types of custom carbon fibres are manufactured by considering three temperature profiles in the low-temperature (LT) and high-temperature (HT) carbonisation ovens. The precursor stabilisation temperatures, the line speed and applied tow tension were kept constant, and identical to those used in the medium tension (MT) trial by Xu et al..[22] Three carbon fibre types were manufactured and studied. These were made using a cool temperature profile (CP), an intermediate temperature profile (IP), and a warm temperature profile (WP). The analyses of the manufactured carbon fibres provide further understanding on how the carbonisation process affects the multifunctional performance of carbon fibres. Understanding how the pulling tension, and the carbonisation temperature influence the mechanical and electrochemical properties of carbon fibres will potentially allow realisation of structural battery composites with significantly improved multifunctional performance.

Results and Discussion

Physical Properties

The physical properties measured for all the manufactured carbon fibres are presented in Table 1. In addition, values for commercial fibres, as reported by the suppliers and in literature are included for comparison.

For all manufactured carbon fibre types, comparable values of density, fibre diameter, electrical conductivity and surface area were obtained. Density and electrical conductivity values are also comparable to those of commercially available carbon fibres. Significantly larger diameters (approximately 7.5 vs. 5 μm) were obtained for the fibres manufactured in this study compared to the commercial IM carbon fibres, possibly due to the use of larger diameter precursor.[23] The surface area measured for the produced carbon fibres is more than two times larger than that of the studied commercial IM carbon fibres. The reason for this difference is also related to the choice of the specific PAN precursor.[24] Nevertheless, the values are still very low compared to other types of surface-modified carbon fibres.[25]

The much smaller surface area for commercial IM carbon fibres is also evident when comparing the SEM images of the manufactured carbon fibres (Figure 1a and Figure S1) with T800 and IMS65 carbon fibres (Figure 1b–c).

X-Ray Photoelectron Spectroscopy (XPS)

The surface chemistry of the manufactured carbon fibres was investigated using X-ray Photoelectron Spectroscopy (XPS). The

Research Article
doi.org/10.1002/batt.202400110
Chemistry Europe
European Chemical Societies Publishing

Table 1. Physical properties for the manufactured carbon fibres and commercially available IM carbon fibres.

Carbon fibre	Density [g cm^{-3}]	Fibre diameter [µm]	Electrical conductivity [S cm^{-1}]	Surface area [m^2 g^{-1}]
Cool profile (CP fibres)	1.793 ± 0.004	7.50 ± 0.64	675.48 ± 87.52	1.17
Intermediate profile (IP fibres)	1.783 ± 0.003	7.71 ± 0.72	724.24 ± 58.62	0.96
Warm profile (WP fibres)	1.786 ± 0.008	7.82 ± 0.64	697.10 ± 124.70	1.13
IMS65	1.780[26]	5.00[26]	689.66[26]	0.42[16]
T800	1.800[27]	5.00[27]	714.29[27]	0.52[16]

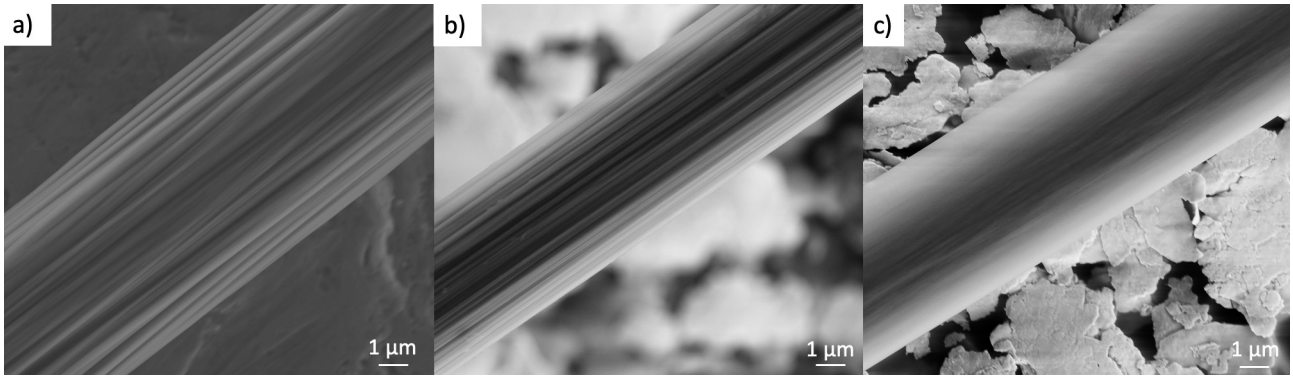

Figure 1. Surface image of the manufactured carbon fibre and comparison with commercially available IM carbon fibres. (a) Cool profile (CP), (b) IMS65, and (c) de-sized T800 carbon fibres.

chemical composition at the surface for the different fibre types is shown in Table 2. The elements which gave the most significant contribution to the spectrum intensity are reported. These elements are thought to be the most relevant ones when evaluating the electrochemical capacity of carbon fibres.[18,28] The obtained spectra are shown in Figure S3.

From the obtained results a change in the chemical composition on the fibre surface with processing temperature is observed. For the manufactured carbon fibres, increasing the temperature during the carbonisation step leads to an increase in carbon content while simultaneously leading to a decrease in the oxygen and nitrogen content. For commercially available carbon fibres, the chemical composition is reported in the manufacturer's data sheet and in previous literature with carbon contents of above 96 %.[17]

Wide-Angle X-Ray Scattering (WAXS)

The microstructure of the manufactured carbon fibres was analysed in equatorial direction. The radial integration of extracted scattering intensity provided information about the crystallite height L_c and d-spacing, while the preferential crystallite orientation relative to the fibre axis was extracted from azimuthal data. The WAXS results presented in Table 3 provide information on the microstructure of the three manufactured carbon fibre types and how it is affected by a change in the carbonisation temperature.[29]

From the data obtained from radial integration, a slight increase in the crystallite height and reduction in d-spacing is observed with increased carbonisation temperatures. From the data obtained along the azimuthal direction, a slight increase in the azimuthal angle with an increase in temperature is found. These findings are in line with what was previously reported in

Table 2. Chemical composition for the considered carbon fibre types obtained from XPS analyses in atomic percentage.

Carbon fibre	Carbon content [%]	Oxygen content [%]	Nitrogen content [%]
Cool profile (CP fibres)	90.4	6.4	3.2
Intermediate profile (IP fibres)	94.4	4.2	1.3
Warm profile (WP fibres)	95.2	3.9	0.8

Research Article
doi.org/10.1002/batt.202400110

Table 3. WAXS analysis results for the three manufactured carbon fibre types.

Carbon fibre	Crystallite height L_c [nm]	d-spacing [Å]	Azimuthal angle [°]
Cool profile (CP fibres)	1.62	3.55	37.61
Intermediate profile (IP fibres)	1.72	3.50	37.78
Warm profile (WP fibres)	1.77	3.44	38.37

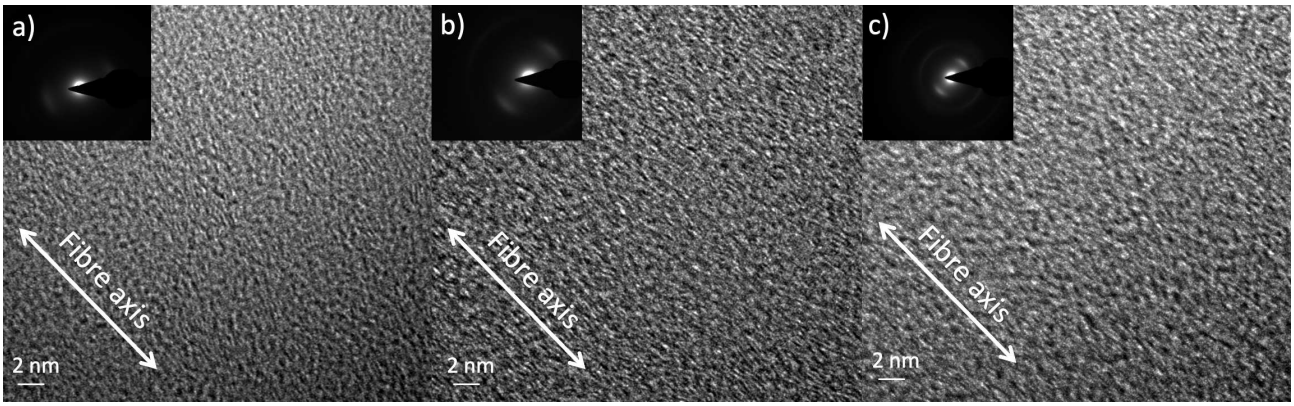

Figure 2. TEM micrographs of the manufactured carbon fibres with white boxes identifying some of the crystalline domains. (a) Cool profile (CP), (b) intermediate profile (IP), (c) warm profile (WP).

the literature for the carbonisation process of carbon fibres.[30] The results from the WAXS analysis can be explained by considering that an increase in the carbonisation temperature will encourage the formation of larger crystals. WAXS spectra are presented in Figure S4.

Transmission Electron Microscopy (TEM)

TEM micrographs were obtained along the fibre axis for the three manufactured carbon fibre types. No significant differences were found in the microstructure close to the surface and in the middle of the fibres. TEM micrographs and diffraction patterns obtained close to the surface for all fibres are shown in Figure 2. All the carbon fibres show small crystallites (brighter areas) aligned along the fibre axis (indicated by the inscribed white arrows). These crystallites are smaller than previously found for commercial IM carbon fibres.[17] The crystallites also show the individual graphene layers distanced by the stacking distance (or d-spacing). Additionally, the micrographs show a high degree of disorder for all the samples and a significant amount of amorphous regions between the crystalline domains characterised by smooth areas. The similarity in the crystallite size observed in the micrographs further confirms the results from the WAXS analyses. The d-spacing between the graphene layers can also be evaluated using the high-resolution TEM micrographs. However, it only represents a rather limited volume. Additionally, in our case, the small crystallite size makes it difficult to obtain reliable values. For larger crystallite sizes like the ones found in commercially available IM and HM carbon fibres, the d-spacing has been previously measured from TEM micrographs.[17] A slight increase in the microstructural order can be seen in the diffraction pattern for the carbon fibre manufactured at higher temperatures. In the earlier study by Xu et al., porous regions were identified close to the surface for all fibres manufactured for different tension forces during stabilisation.[22] This is not confirmed here. In the current study, pores were only found close to the surface for the fibre type manufactured by the warm profile. Furthermore, pores were only found on the far side (the side farther away from the Pt coating) (Figure S2).

Mechanical Properties

The mechanical properties measured for the manufactured carbon fibres are presented in Table 4. For comparison values for IMS65 and T800 were measured with the same method and are included in the table.

The carbon fibres manufactured at higher carbonisation temperatures, i.e., IP and WP fibres, exhibit the highest elastic modulus and tensile strength. However, the tensile modulus of the manufactured fibres is 12% to 15% lower, and the tensile strength is 20% to 25% lower, than for the commercial IMS65 and T800 IM carbon fibres. The tensile strength in particular, is reduced for larger cross-sections, due to the higher chances of having defects after the manufacturing.

Research Article
doi.org/10.1002/batt.202400110
Chemistry Europe
European Chemical Societies Publishing

Table 4. Mechanical properties for the manufactured carbon fibres and commercially available IM carbon fibres.

Carbon fibre	Tensile modulus [GPa]	Tensile strength [GPa]	Strain to failure [%]
Cool profile (CP fibres)	204.45 ± 7.34	2.81 ± 0.62	1.44 ± 0.31
Intermediate profile (IP fibres)	213.74 ± 14.94	2.85 ± 0.66	1.41 ± 0.29
Warm profile (WP fibres)	212.00 ± 8.12	3.02 ± 0.66	1.51 ± 0.30
IMS65	247.14 ± 8.79	4.28 ± 0.89	1.85 ± 0.36
T800	241.35 ± 3.39	3.85 ± 0.66	1.70 ± 0.27

The considered temperatures for the high-temperature carbonisation step seem to have only a marginal effect on the tensile performances of the manufactured carbon fibres. A similar behaviour is found for the physical properties. This is most likely due to the high-temperature carbonisation leading to only slight microstructural changes. Mechanical properties are known to be affected by crystallite size and orientation.[10,17] However, the observed variability in the carbonaceous microstructure from WAXS spectra and TEM micrographs is too small to justify significant differences in mechanical properties between the manufactured carbon fibre types.

Electrochemical Properties

The electrochemical properties measured for the manufactured carbon fibres, as well as the two commercial IM carbon fibres, are presented in Table 5. Voltage profiles for both lithiation and delithiation for the 1st and 10th lithiation cycle for the three manufactured carbon fibres are depicted in Figure 3a–c. The fibres show good reversibility in the capacity after the first lithiation cycle. In Figure 3d–f the effect of the C-rate is shown for the three manufactured carbon fibre types. Cyclic voltammograms are shown in Figure S5 .

Differences in the 1st cycle capacity were found between the three manufactured carbon fibre types. Higher carbonisation temperatures result in lower first-cycle capacity. In contrast, the carbonisation temperature did not affect the first cycle capacity loss percentage. A first-cycle capacity loss of 39% was found for all manufactured carbon fibre types. The 10th cycle capacity showed a similar trend to the 1st cycle capacity, but the difference between the three fibre types is smaller. The behaviour for cycles after the 10th cycle at different C-rates was similar to that of the 1st cycle for the three manufactured carbon fibres. Higher 1st and 10th cycle capacities were measured for the three manufactured carbon fibre types compared to the commercial ones. However, the 1st cycle losses were smaller for the commercial fibres. The higher 1st cycle loss for the manufactured carbon fibre types is likely associated with their larger surface area. The obtained values for the first cycle losses are higher than in conventional battery materials but are in line with what was observed in other works focused on structural battery electrolytes.[16,22] This behaviour is due to the combination of solid electrolyte interphase (SEI) formation (as in graphite electrodes) and trapped lithium inside of the carbon fibre turbostratic structure. In fact, as reported by Johansen et al., around 25% of the capacity loss for intermediate-modulus carbon fibres is caused by lithium ions trapped.[31] Furthermore, the results of the electrochemical characterisation are confirmed by the microstructural analysis findings, with smaller crystallites and d-spacing leading to higher electrochemical performance. The effect of the carbonisation temperature on the crystallite size and subsequently on the electrochemical capacity has previously been reported by Fredi et al. when comparing the electrochemical behaviour of commercially available carbon fibres.[17] High-modulus carbon fibres (which are carbonised at temperatures up to 3000 °C) showed crystallite sizes one order of magnitude larger than intermediate-

Table 5. Electrochemical cycling results for the manufactured carbon fibres and commercially available IM carbon fibres.

Carbon fibre	1st cycle capacity [mAh g^{-1}]	10th cycle capacity [mAh g^{-1}]	1st cycle loss [mAh g^{-1}]	1st cycle loss [%]	10th cycle CE [%]
Cool profile (CP fibres)	342	158	140	39	99.99
Intermediate profile (IP fibres)	321	152	126	39	99.83
Warm profile (WP fibres)	295	146	115	39	99.95
IMS65	318	141	109	34	98.74
T800	266	142	84	32	98.94

Research Article
doi.org/10.1002/batt.202400110
Chemistry Europe
European Chemical Societies Publishing

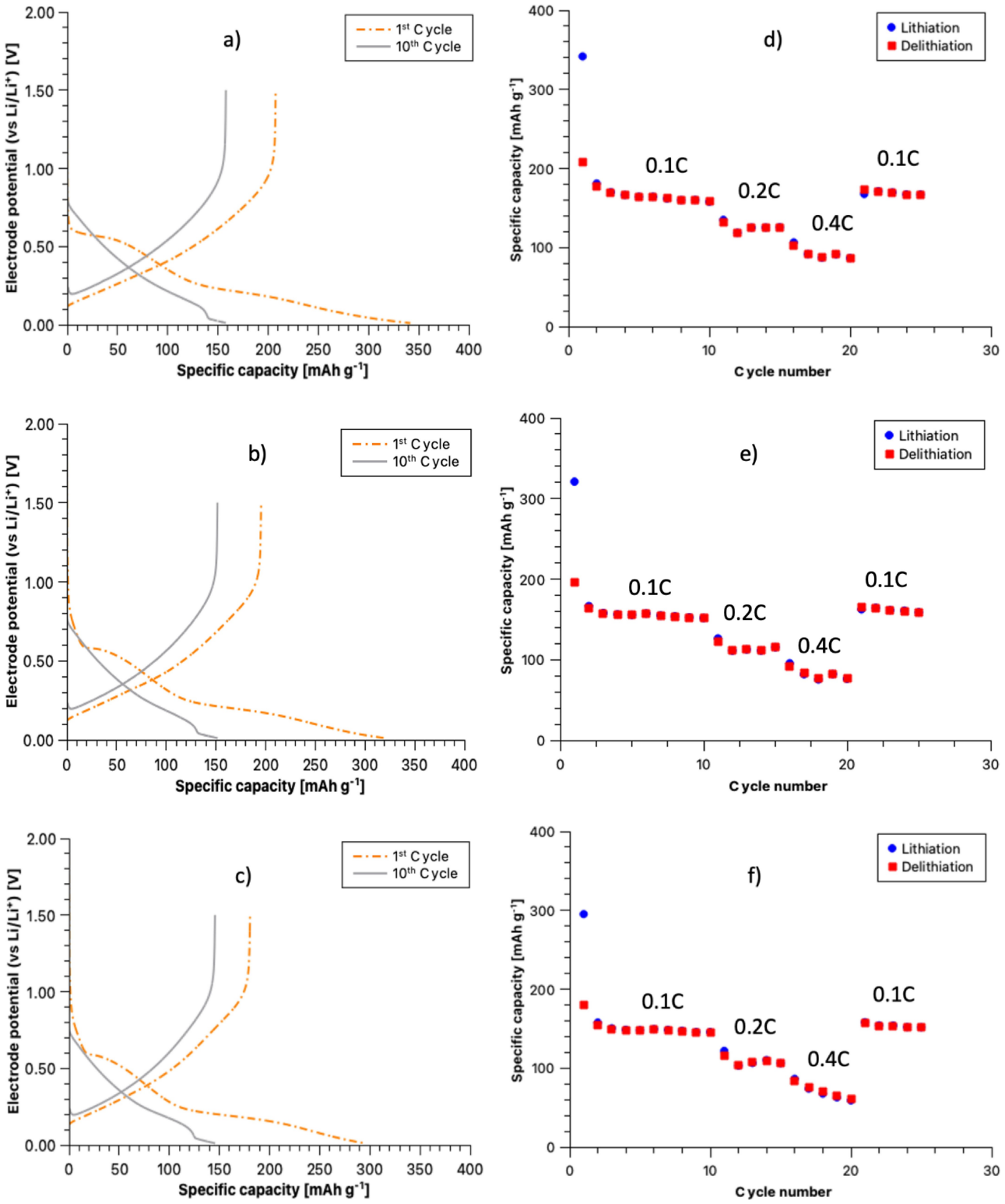

Figure 3. Charge/discharge profiles for the 1st and 10th cycle at 0.1 C rate for (a) cool profile (CP), (b) intermediate profile (IP), and (c) warm profile (WP) carbon fibres. Specific capacities for lithiation and delithiation at different current densities corresponding to 0.1 C, 0.2 C, 0.4 C and 0.1 C for (d) CP, (e) IP, and (f) WP carbon fibres.

modulus carbon fibres (which are carbonised at temperatures up to 1600 °C). These changes in crystallite size were then translated into higher electrochemical capacities for the carbon fibres with the smallest crystallites. The same behaviour is observed in the current study.

Research Article
doi.org/10.1002/batt.202400110
Chemistry Europe
European Chemical Societies Publishing

Previous studies by Johansen et al., utilizing Auger electron spectroscopy to map lithium insertion in carbon fibres, revealed a uniform distribution of lithium within the fibres.[28] The TEM micrographs (Figure 2) complement these findings by illustrating the uniform distribution of both amorphous and crystalline domains. It has been reported that for materials like the considered carbon fibres, characterised by a turbostratic microstructure and small crystallites, the lithium insertion mechanism is similar to that of amorphous carbon with the difference that some lithium intercalation can still happen in the graphitic regions.[28] In this model, called single-layer model, the presence of amorphous regions around the disordered crystalline domains hinders the intercalation.[32] The lithium ions will mainly be stored in the amorphous parts of the carbon fibre as well as in the proximity of defects like nanocavities. Furthermore, the presence of specific heteroatoms, like pyridinic and pyrrolic nitrogen, has been found to increase the capacity of carbon fibres.[18,33] This highlights the significance of not only considering the crystalline domain but also recognizing the role of amorphous regions. While discussions on graphite as an electrode material typically concentrate on crystal structure, particularly crystallite size, the WAXS results of our study align with this focus by emphasizing the favourable nature of a smaller crystallite height. Moreover, this work demonstrates that the combined effect of overall smaller crystalline domains in the material, coupled with a larger d-spacing as for the CP fibre, results in a higher electrochemical storage capacity. Furthermore, slightly increased coulombic efficiency was measured for the manufactured carbon fibres, compared to commercial IM carbon fibres. It should be noted that the coulombic efficiency measured for the T800 and IMS65 carbon fibres in this study is lower than what was previously reported by Hagberg et al., who reported coulombic efficiency for the commercial IM fibres on par with the manufactured carbon fibre types studied here.[16] Long-term cycling has not been performed in the current study as we followed the same procedure used in an earlier study, focusing on the coulombic efficiency.[22] Long-term cycling will be performed once the manufactured carbon fibres will be used in structural full cell where the longevity on a system level is a key factor. Additionally, the results from the XPS analysis show that different chemical compositions are obtained on the surface, indicating that the different manufacturing parameters are effectively altering the carbon fibre composition. This difference likely plays a role in the first cycle losses where most of the SEI is being formed. The cyclic voltammograms for the manufactured carbon fibres are shown in Figure S5. A slight anodic peak shift for the different manufactured carbon fibres is clearly visible. Cyclic voltammograms for the commercially available carbon fibres have been previously reported in literature.[15]

Multifunctional Performance

The results demonstrate a clear, but moderate, impact of the carbonisation temperature profile on multifunctionality. In particular, lithium storing capabilities are affected by the chosen carbonisation temperature. This is explained by the smaller crystallite size and a larger d-spacing found for the fibre types with reduced carbonisation temperature.[34] In addition, the electrochemical capacity is further increased by the larger amount of amorphous domains in these carbon fibres.[17,23] Conversely, the change in the microstructure and cross-section size leads to lower mechanical properties than those of the commercial IM carbon fibres. The multifunctionality of the three carbon fibre types made in this study is displayed in Figure 4 plotting the tensile strength and elastic modulus against the 10th cycle capacity.The multifunctional properties of the carbon fibres produced here are somewhat lower than those previously reported by Xu et al. using the same precursor material and manufacturing facilities, but processed at slightly higher carbonisation temperatures.[22] Furthermore, different liquid electrolytes were used in the half-cells manufactured and galvanostatically cycled in the two studies. Even though the

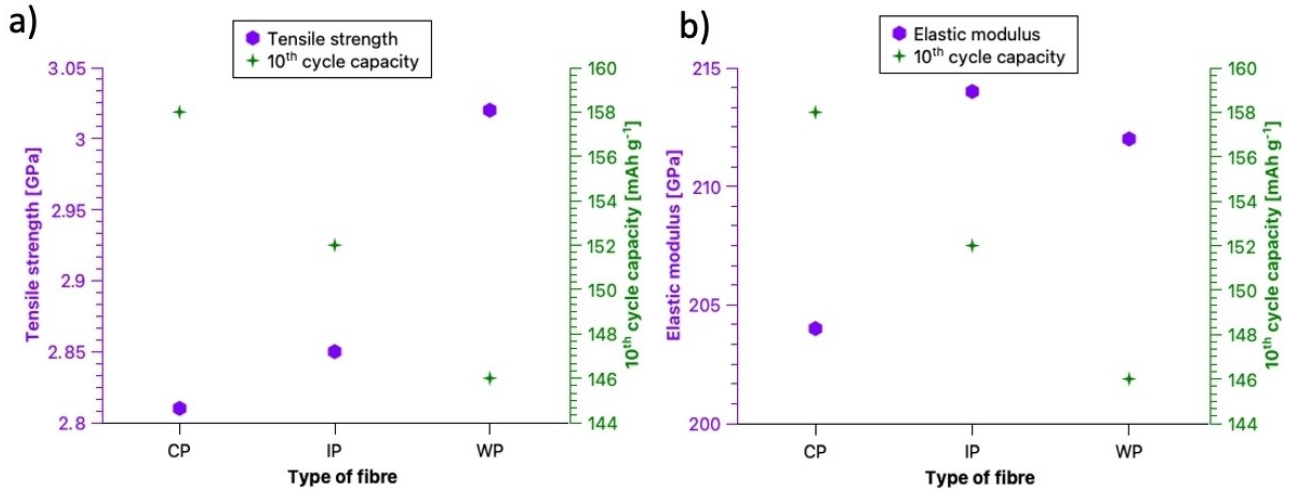

Figure 4. Multifunctionality of the three manufactured carbon fibre types with respect to (a) tensile strength and 10th cycle capacity, and (b) elastic modulus and 10th cycle capacity.

results from the two studies cannot be directly compared due to the aforementioned differences, effects of tension force during stabilization and carbonization temperature during carbonization on fibre multifunctional performance have been demonstrated. Thus, the two studies combined, provide guidance for manufacture of multifunctional carbon fibres within a moderate design space considering fibre modulus and strength and combined electrochemical capacity.

Conclusions

In this study, the effect of carbonisation temperature profiles on the carbonaceous microstructure and multifunctional performance of carbon fibres is investigated. PAN-based fibre precursors and carbonisation temperatures commonly used for realisation of intermediate modulus carbon fibres are explored. Low to high temperature profiles are studied and found to have small to moderate effect on the achieved fibre microstructure and multifunctionality. Elastic modulus and tensile strength of the fibres were found to decrease by up to 7% whereas the electrochemical capacity increased by close to 15% as the processing temperature was reduced from the high-temperature profile to the low-temperature profile. For these fibres, electrochemical capacity is marginally improved compared to commercially available IM carbon fibres (up to 11%) but the mechanical properties are reduced at the same time (up to 15% for the tensile modulus and 25% for the tensile strength). The changes in multifunctional performance are related to differences in the achieved graphitic microstructure. The results from this study and the previous study by Xu et al.,[22] imply that for PAN-based carbon fibres with properties similar to commercial IM carbon fibres, the multifunctionality window which can be achieved is narrow. In order to significantly extend the multifunctional design envelope of carbon fibres a much wider processing window for carbon fibre manufacturing will be required.

Experimental Section

Materials

Carbon fibres were manufactured at Carbon Nexus, Institute for Frontier Materials, Deakin University (Australia) on a research line equipped with advanced production technologies (Despatch Industries, USA; Furnace Engineering Pty Ltd, Australia).

A 24 K tow of polyacrylonitrile (PAN) fibres (Bluestar Ltd, China) was used as precursor. The precursor fibres were stabilised in 4-zone oxidation ovens at temperatures ranging from 228 °C to 258 °C. Three different temperature profiles are considered after the oxidation step for the manufacture of the three different carbon fibre versions, as shown in Table 6 below. For the sake of clarity, the trials have been named cool profile (CP) for the lower temperature profile, intermediate profile (IP) for the medium temperature profile, and warm profile (WP) for the higher temperature profile. In the research line used for this work, the low-temperature carbonisation furnace (LT-furnace) has three temperature zones, while the high-temperature carbonisation furnace (HT-furnace) has two temperature zones.

The line speed was set to 30 m/h leading to a duration of 2.5 and 2.3 minutes for the low-temperature and high-temperature carbonisation steps, respectively. The average tension applied to the fibres during the oxidation step was 2300 cN. The average tension applied to the fibres during low-temperature and high-temperature carbonisation for all the trials was 1200 cN and 1700 cN, respectively. Carbon fibres were extracted after the high-temperature carbonisation furnace and collected on a winder. A schematic illustration of the carbon fibre manufacturing process is presented in Figure 5.

Characterisation of Physical Properties

Fibre diameter was measured by automated optical laser image analysis using a CottonscopeHD instrument (Diamscope, Australia). Approximately 5000 fibre fragments were measured for each carbon fibre type to obtain a fibre diameter distribution. Density was obtained using a density gradient column in accordance with ASTM D1505-10. Three different samples were measured for each carbon fibre type.

Electrical conductivity was measured using a 4-point probe setup.[35] Ten different samples were considered for each carbon fibre type.

Surface area was measured by Brunauer-Emmett-Teller (BET) surface area analysis using an inverse gas chromatography surface energy analyser, iGC-SEA (Surface Measurement Systems, UK) through octane gas adsorption at 30 °C. The surface of the carbon fibres was also investigated using a field emission scanning electron microscope LEO-1550 (Zeiss, Germany).

Characterisation of Mechanical Properties

The elastic modulus, tensile strength and strain to failure were measured using a single fibre tensile testing machine, Favimat+ (Textechno, Germany), with a 210 cN load cell and a gauge length of 20 mm. The single carbon fibre filaments were tested according to ASTM D 3822-07 with a pulling speed of 1 mm/min. Fifty samples were tested for each carbon fibre type. In addition, mechanical properties of the commercial IM carbon fibres (IMS65 and T800) were measured following the same procedure.

Table 6. Different temperature profiles adopted for the three carbon fibre versions.

Temperature profile	LT-furnace zone 1 [°C]	LT-furnace zone 2 [°C]	LT-furnace zone 3 [°C]	HT-furnace zone 1 [°C]	HT-furnace zone 2 [°C]
Cool profile (CP fibres)	284	450	600	1000	1300
Intermediate profile (IP fibres)	350	550	700	1100	1400
Warm profile (WP fibres)	450	650	800	1200	1500

Research Article
doi.org/10.1002/batt.202400110
Chemistry Europe
European Chemical Societies Publishing

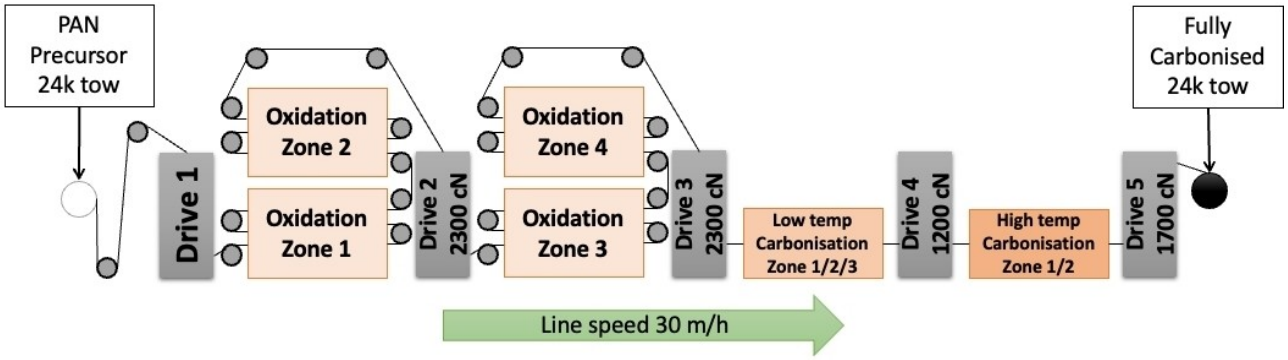

Figure 5. Schematic of the manufacturing line. Precursor fibres enter the four oxidation ovens and then enter the low-temperature carbonisation and the high-temperature carbonisation furnaces. Pulling drives are distributed along the line to ensure strict control on the applied tensions. The carbon fibres are collected on a winder at the end of the line.

Characterisation of Electrochemical Properties

Electrode samples were made from 24 K tows for each carbon fibre type. In addition, electrode samples were made from commercial IMS65 and T800 fibres. Here, 24 K tows of the unsized IMS65 fibres and two 12 K tows of the de-sized T800 fibres were used, respectively. Copper strip current collectors were attached to the carbon fibre tows using silver paint. The samples were dried at 50 °C in vacuum overnight prior to cell assembly in an argon-filled glove box (<1 ppm H_2O and O_2).

The electrochemical characterisation of the fibres was performed using a two-electrode pouch cell. A lithium metal foil acted as the counter and reference electrode, a 260 μm thick glass microfiber layer (Whatman GF/A) acted as the separator, and a solution of 1.0 M lithium bis(trifluoromethanesulfonyl)imide (LiTFSI) salt in a 1 : 1 by weight mixture of ethylene carbonate and propylene carbonate (EC:PC) was used as electrolyte. Galvanostatic charge/discharge cycling was performed to measure specific capacity, first cycle losses, and coulombic efficiency of the carbon fibre electrodes. These tests were done using a Neware CT-4008-5V10mA-164 battery cycler.

Additionally, cyclic voltammetry was used to determine the impact of the fibre type on the lithium insertion process. Identical two-electrode pouch cells as previously mentioned were used. A voltage between 0.05 V and 3 V was used with a sweep rate of 1 $mV\,s^{-1}$. All measurements were performed using a Bio-Logic BCS 805 station.

The half-cells were cycled between 0.01 V and 1.50 V vs Li/Li^+, and the currents used corresponded to current densities of 0.1 C, 0.2 C, and 0.4 C, based on graphite's theoretical maximum capacity of 372 $mAh\,g^{-1}$. The cycling sequence consisted of ten cycles at 0.1 C, five cycles at 0.2 C, five cycles at 0.4 C, and five cycles at 0.1 C. A two-hour resting time was considered after every charging/discharging phase. Three samples were tested for each fibre type. The average mass of the active materials, the linear density, and currents are shown in Table 7.

X-Ray Photoelectron Spectroscopy (XPS)

XPS measurements were performed using a ULVAC-PHI PHI5000 VersaProbe III Scanning X-ray Microprobe instrument with monochromatized Al Kα radiation (1486.7 eV). The x-ray beam was set to a spot size of 100 μm. A total of 10 sweeps were completed for each sample for each evaluated spot. The pass energy was set to 26 eV with a step time of 10 ms and a step size of 0.1 eV. A range between 0 eV and 1350 eV was investigated. The samples were attached on a sample holder plate with the surface facing the x-ray source using adhesive copper tape. The MultiPak software was used to conduct peak deconvolution of XPS data.

Wide-Angle X-Ray Scattering (WAXS)

WAXS measurements were performed at the Institute for Frontier Materials, Deakin University (Australia) using a Xeuss 3.0 beamline with an X-ray beam energy of 9 keV. The sample-to-detector distance was set to 600 mm with an exposure time of 360 s. Carbon fibre samples consisting of small bundles of five single fibre filaments were attached to a 3D-printed sample holder in vertical orientation and positioned perpendicular to the incident beam. The sample holder was free to move on an X–Y linear stage inside the vacuum chamber. The obtained scattering patterns along the equatorial direction were reduced to a series of X–Y plots with the

Table 7. Average active masses and cycling currents.

Carbon fibre	Mass [g]	Linear density [$g\,cm^{-1}$]	Current at 0.1 C [mA]	Current at 0.2 C [mA]	Current at 0.4 C [mA]
Cool profile (CP fibres)	0.0761	0.0152	2.82	5.64	11.28
Intermediate profile (IP fibres)	0.0779	0.0156	2.94	5.87	11.74
Warm profile (WP fibres)	0.0738	0.0148	2.73	5.45	10.91
IMS65	0.0324	0.0065	1.23	2.46	4.91
T800	0.0397	0.0079	1.43	2.86	5.73

scattering angle (q) plotted against the X-ray intensity using an integration along the equatorial direction, with an azimuthal angle of $\pm 2°$. The peaks from the obtained plots were fitted with a pseudo-Voigt function.[36] The full width at half maximum (FWHM) of the fitted curve's peak was used to determine the crystallite size L_c, using Scherrer's equation.[37] The peak position was used to determine the d-spacing of the lattice according to Bragg's law.[38]

The scattering patterns along the azimuthal direction were then analysed to determine the crystallite's preferential orientation. These patterns were reduced to a series of X–Y plots with the azimuthal angular position (φ) plotted against the X-ray intensity. The peaks from the obtained plots were fitted with a Gaussian function and the FWHM of the fitted curve's peak was used to determine an orientation factor.

Transmission Electron Microscopy (TEM)

TEM was used to investigate the microstructure of the manufactured carbon fibres. For this purpose, approximately 100 nm thick samples, with parallel surfaces were prepared using a procedure previously employed by Fredi et al. in the microstructural characterisation of the commercial IM carbon fibres.[17] Sample preparation was performed in a focused ion beam and scanning electron microscope (FIB/SEM) using an in-situ lift-out technique. Here, a Versa 3D DualBeam FIB/SEM instrument equipped with a gallium (Ga) ion source for ion milling, an injection system for platinum (Pt) deposition, and a micro-manipulation system (Omniprobe) was used. As previously reported, the in-situ lift-out procedure starts with the deposition of a Pt layer (100 nm deposited using the electron beam and 1 μm deposited using the ion beam) to preserve the sample from ion damage in the subsequent steps.[39,40] SEM images of the sample preparation are presented in Figure S6. After the sample is cut free from the initial carbon fibre it is later attached to the TEM holder and is thinned down via multiple steps until a thickness of approximately 100 nm is obtained. An ion beam at 30 kV accelerating voltage is initially used; while for the final steps, polishing using 5 kV and 2 kV is performed to minimize the ion induced damage to the surface. A FEI Titan 80-300 TEM was used to analyse the microstructure of the thin carbon fibre samples with an accelerating voltage of 300 kV. No changes were observed in the materials during the analysis.

Acknowledgements

The authors would like to thank the following entities for funding this research: United States Air Force (USAF), USA, Award Number FA8655-21-1-7038, Office of Naval Research (ONR), USA, Award Numbers N62909-22-1-2037 and N62909-22-1-2052, Swedish National Space Agency, Contract 2020-00256, Swedish Energy Agency, Contract 46598-1, 2D TECH VINNOVA Competence Center, Contract 2019-00068. This work was partly performed at the Chalmers Material Analysis Laboratory (CMAL). The authors would also like to thank Mr. John Herron, Dr. Maxime Maghe and Mr. Scott Anderson at Carbon Nexus for manufacturing the carbon fibres analysed in the current study.

Conflict of Interests

The authors declare no conflict of interest.

Data Availability Statement

The data that support the findings of this study are available from the corresponding author upon reasonable request.

Keywords: batteries carbon fibres · multifunctional materials · carbon fibre composites · structural batteries

[1] L. E. Asp, E. S. Greenhalgh, *Compos. Sci. Technol.* **2014**, *101*, 41–61.
[2] L. E. Asp, M. Johansson, G. Lindbergh, J. Xu, D. Zenkert, *Funct. Compos. Struct.* **2019**, *1*, 042001.
[3] T. Jin, G. Singer, K. Liang, Y. Yang, *Mater. Today* **2023**, *62*, 151–167.
[4] W. Johannisson, D. Zenkert, G. Lindbergh, *Multifunct. Mater.* **2019**, *2*, 035002.
[5] C. Meng, N. Muralidharan, E. Teblum, K. E. Moyer, G. D. Nessim, C. L. Pint, *Nano Lett.* **2018**, *18*, 7761–7768.
[6] K. Moyer, C. Meng, B. Marshall, O. Assal, J. Eaves, D. Perez, R. Karkkainen, L. Roberson, C. L. Pint, *Energy Storage Mater.* **2020**, *24*, 676–681.
[7] W. Ruland, *Adv. Mater.* **1990**, *2*, 528–536.
[8] J. F. Snyder, E. L. Wong, C. W. Hubbard, *J. Electrochem. Soc.* **2009**, *156*, A215.
[9] S.-J. Park, in *Carbon Fibers* (Ed.: S.-J. Park), Springer, Singapore, **2018**, pp. 31–67.
[10] D. J. Johnson, *J. Phys. D* **1987**, *20*, 286–291.
[11] E. Jacques, M. H. Kjell, D. Zenkert, G. Lindbergh, *Carbon* **2014**, *68*, 725–733.
[12] E. Jacques, M. Hellqvist Kjell, D. Zenkert, G. Lindbergh, M. Behm, *Carbon* **2013**, *59*, 246–254.
[13] E. Jacques, M. H. Kjell, D. Zenkert, G. Lindbergh, M. Behm, M. Willgert, *Compos. Sci. Technol.* **2012**, *72*, 792–798.
[14] S. Duan, A. H. S. Iyer, D. Carlstedt, F. Rittweger, A. Sharits, C. Maddox, K.-R. Riemschneider, D. Mollenhauer, M. Colliander, F. Liu, L. E. Asp, *Carbon* **2021**, *185*, 234–241.
[15] M. H. Kjell, E. Jacques, D. Zenkert, M. Behm, G. Lindbergh, *J. Electrochem. Soc.* **2011**, *158*, A1455.
[16] J. Hagberg, S. Leijonmarck, G. Lindbergh, *J. Electrochem. Soc.* **2016**, *163*, A1790.
[17] G. Fredi, S. Jeschke, A. Boulaoued, J. Wallenstein, M. Rashidi, F. Liu, R. Harnden, D. Zenkert, J. Hagberg, G. Lindbergh, P. Johansson, L. Stievano, L. E. Asp, *Multifunct. Mater.* **2018**, *1*, 015003.
[18] M. Johansen, C. Schlueter, P. L. Tam, L. E. Asp, F. Liu, *Carbon* **2021**, *179*, 20–27.
[19] L. E. Asp, K. Bouton, D. Carlstedt, S. Duan, R. Harnden, W. Johannisson, M. Johansen, M. K. G. Johansson, G. Lindbergh, F. Liu, K. Peuvot, L. M. Schneider, J. Xu, D. Zenkert, *Adv Energy Sustain Res* **2021**, *2*, 2000093.
[20] J. Xu, Z. Geng, M. Johansen, D. Carlstedt, S. Duan, T. Thiringer, F. Liu, L. E. Asp, *EcoMat* **2022**, *4*, DOI 10.1002/eom2.12180.
[21] M. S. Siraj, S. Tasneem, D. Carlstedt, S. Duan, M. Johansen, C. Larsson, J. Xu, F. Liu, F. Edgren, L. E. Asp, *Adv. Energy Sust. Res* **n.d.**, *n/a*, 2300109.
[22] J. Xu, C. Creighton, M. Johansen, F. Liu, S. Duan, D. Carlstedt, P. Mota-Santiago, P. Lynch, L. E. Asp, *Carbon* **2023**, *209*, 117982.
[23] M. Minus, S. Kumar, *JOM* **2005**, *57*, 52–58.
[24] Y.-P. Jeon, R. Alway-Cooper, M. Morales, A. A. Ogale, in *Handbook of Advanced Ceramics (Second Edition)* (Ed.: S. Somiya), Academic Press, Oxford, **2013**, pp. 143–154.
[25] C. Liu, L. Miao, R. Zhao, F. Yang, V. Unnikrishnan, R. Rana, N. Deng, M. R. Ghandehari Ferdowsi, Q. Chao, W. Kang, J. M. Razal, L. Miao, M. Naebe, Q. Li, *Carbon* **2022**, *193*, 368–380.
[26] "Filament Yarn: Teijin Carbon: Teijin Carbon," can be found under https://www.teijincarbon.com/products/filament-yarn/, **n.d**.
[27] *Toray Composite Materials America, Inc.* can be found at https://www.toraycma.com/wp-content/uploads/T800H-Technical-Data-Sheet-1.pdf, **n.d.**.
[28] M. Johansen, J. Xu, P. L. Tam, L. E. Asp, F. Liu, *Appl. Surf. Sci.* **2023**, *627*, 157323.
[29] M. Guigon, A. Oberlin, G. Desarmot, *Fibre Sci. Technol.* **1984**, *20*, 177–198.
[30] R. Shokrani Havigh, H. Mahmoudi Chenari, *Sci. Rep.* **2022**, *12*, 10704.
[31] M. Johansen, M. P. Singh, J. Xu, L. E. Asp, B. Gault, F. Liu, *Carbon* **2024**, *225*, 119091.

[32] M. Endo, Y. A. Kim, in *Carbon Alloys* (Eds.: E. Yasuda, M. Inagaki, K. Kaneko, M. Endo, A. Oya, Y. Tanabe), Elsevier Science, Oxford, **2003**, pp. 417–433.
[33] T. Wu, M. Jing, Y. Tian, L. Yang, J. Hu, X. Cao, G. Zou, H. Hou, X. Ji, *Adv. Funct. Mater.* **2019**, *29*, 1900941.
[34] M. Endo, Y. Nishimura, T. Takahashi, K. Takeuchi, M. S. Dresselhaus, *J. Phys. Chem. Solids* **1996**, *57*, 725–728.
[35] K. H. Wong, S. J. Pickering, C. D. Rudd, *Composites Part A* **2010**, *41*, 693–702.
[36] A. Gibaud, S. Hazra, *Curr. Sci.* **2000**, *78*, 1467–1477.
[37] S. Nunna, M. Naebe, N. Hameed, C. Creighton, S. Naghashian, M. J. Jennings, S. Atkiss, M. Setty, B. L. Fox, *Polym. Degrad. Stab.* **2016**, *125*, 105–114.
[38] D. D. Le Pevelen, in *Encyclopedia of Spectroscopy and Spectrometry (Second Edition)* (Ed.: J. C. Lindon), Academic Press, Oxford, **2010**, pp. 2559–2576.
[39] R. M. Langford, C. Clinton, *Micron* **2004**, *35*, 607–611.
[40] S. Duan, F. Liu, T. Pettersson, C. Creighton, L. E. Asp, *Carbon* **2020**, *158*, 772–782.

Manuscript received: February 19, 2024
Revised manuscript received: April 16, 2024
Accepted manuscript online: May 16, 2024
Version of record online: June 21, 2024